Planar Microfluidic Chamber for Generation of Stable and Steep Chemoattractant Gradients

Sandra Fok,* Peter Domachuk,† Gary Rosengarten,‡ Norbert Krause,§ Filip Braet,* Benjamin J. Eggleton,† and Lilian L. Soon*

*Australian Microscopy and Microanalysis Research Facility, Australian Key Centre for Microscopy and Microanalysis, The University of Sydney, Sydney, NSW, Australia; ‡School of Mechanical Engineering, University of New South Wales, Sydney, NSW, Australia; †ARC Centre of Excellence for Ultrahigh Bandwidth Devices for Optical Systems, School of Physics, The University of Sydney; and §Bandwidth Foundry, Australian Technology Park, NSW, Australia

ABSTRACT The extracellular availability of growth factors, hormones, chemokines, and neurotransmitters under gradient conditions is required for directional cellular responses such as migration, axonal pathfinding, and tissue patterning. These responses are, in turn, important in disease and developmental processes. This article addresses critical barriers toward devising a chemotaxis assay that is broadly applicable for different kinds of cancer cells through the design of a microfluidic chamber that produces a steep gradient of chemoattractant. Photolithography was used to create microchannels for chemoattractant delivery, flow diversion barriers/conduits, and small outlets in the form of apertures. The 1-μm apertures were made at the active surface by uncapping a thin (1.5 μm) layer of AZ1518. This process also created a vertical conduit that diverted the flow such that it occurred perpendicularly to the active, experimental surface where the gradients were measured. The other side of the vertical conduit opened to underlying 20-μm deep channels that carried microfluidic flows of tracer dyes/growth factors. Modeled data using computational fluid dynamics produced gradients that were steep along the horizontal, active surface. This simulation mirrors empirically derived gradients obtained from the flow analyses of fluorescent compounds. The open chamber contains a large buffer volume, which prevents chemoattractant saturation and permits easy cell and compound manipulation. The technique obviates the use of membranes or laminar flow that may hinder imaging, rinsing steps, cell seeding, and treatment. The utility of the chamber in the study of cell protrusion, an early step during chemotaxis, was demonstrated by growing cancer cells in the chamber, inducing a chemoattractant gradient using compressed air at 0.7 bar, and performing time-lapse microscopy. Breast cancer cells responded to the rapidly developed and stable gradient of epidermal growth factor by directing centroid positions toward the gradient and by forming a leading edge at a speed of 0.45 μm/min.

INTRODUCTION

Chemoattractants such as chemokines and growth factors are important inducers of cell migration. The factors bind and activate cell surface receptors that, in turn, trigger downstream signal pathways that lead to the reorganization of the cytoskeleton and other machineries resulting in cell movement. The directional movement of cells in the presence of a chemoattractant gradient is called ''chemotaxis''. The early response of the cell after receptor activation is the generation of an internal gradient of second messengers that exceed the strength of the external gradient (1–3). This effect is known as ''sensing'' and leads to the polarization of the cell in forming a distinct leading front and trailing edge. The cell adheres to the underlying substrate through integrins followed by actomyosin contraction that releases the cell, propelling it forward (4).

Cell migration occurs in a variety of biological processes such as wound healing, development, and immune responses. In disease processes such as cancer, migration is involved in the spread of the disease or metastasis. Cancer cells have been shown in vivo to actively form protrusions and were migratory in close proximity to blood vessels and host macrophages (5). Subsequent experiments demonstrated a paracrine relationship between the cancer cells that expressed the colony-stimulating factor-1 (CSF-1) ligand and epidermal growth factor receptor (EGFR) and the macrophages that expressed the epidermal growth factor (EGF) ligand and the CSF-1 receptor. The cross-stimulation of the different receptors promoted the migration of these two types of cell (6). Therefore, the nature of the interactions between the cells is within short distances, and the gradients of chemoattractant, such as for EGF, are likely to be steep.

Under in vitro conditions, cancer cells are slow moving compared to other naturally motile cells such as leukocytes. Cancer cells also respond poorly to micropipette assays that create gradients by pressure-driven extrusion of the chemoattractants and to other visual-based chemotaxis assays that are more appropriate for faster moving cells such as neutrophils or more polarized cells (7–9). However, modification of the micropipette assay by restricting the chemoattractant flow to create stable and steep gradients enabled cancer cell chemotaxis (10). In this study, we refined the assay by devising a planar, microfluidic chamber that recreates similar gradients.

Submitted August 1, 2007, and accepted for publication March 18, 2008.

Address reprint requests to Lilian L. Soon, Australian Microscopy and Microanalysis Research Facility (AMMRF), Australian Key Centre for Microscopy and Microanalysis (AKCMM), The University of Sydney, Madsen Building, F09, Room LG14, NSW, 2006, Australia. E-mail: l.soon@usyd.edu.au.

Editor: Cristobal G. dos Remedios.

0006-3495/08/08/1523/08 $2.00

doi: 10.1529/biophysj.107.115246

The transparent device also permits direct viewing with sufficient throughput for experimental analyses.

The processes of creating small, high aspect ratio features in thicker substrates normally require anisotropic plasma etching, which is expensive and which may incur etch bias anomalies. The method described here, which uses a thin (1.5-μm), substrate, works well in the lithographic generation micrometer-size apertures that superimpose over larger microfluidic channels.

The generation of a steep gradient of chemoattractant was verified by modeling and experimental data. Culturing of breast cancer cells, time-lapsed microscopy, and analysis of parameters such as directionality and instantaneous speed of cell protrusion were performed. The data indicated that the cancer cells responded significantly more directionally and rapidly compared to uninduced cells in the presence of an EGF gradient, demonstrating the value of the planar chamber for the evaluation of cancer cell behavior.

MATERIALS AND METHODS

Microfluidic chamber

The planar device (PD) constitutes three sections that were assembled on top of each other and kept under positive pressure in a metal chamber. The bottom layer consists of a glass substrate with patterned polymer microfluidic channels that lead from a reservoir or inlet. A plan-parallel, poly (dimethylsiloxane) (PDMS) (11) seal of 2-mm thickness overlie this layer. It serves to seal the reservoir, define the open tank for extrusion of the chemoattractant and gradient formation, and distribute the pressure on the assembly evenly. A PMMA block sits on top of the PDMS; the block connects to a pressure regulator (0–0.7 bar) at an opening that leads to the reservoir. The whole stack is pressed together in a fitted metal chamber (Fig. 1 *A*).

The active device as such consists of a thin film of an ultraviolet curable epoxy resin (UV15; Master Bond, Hackensack, NJ) with 20-μm channels imprinted by means of photolithography (Fig. 2). To seal the channels, a 1.5-μm thick film of AZ1518 (Clariant, Muttenz, Switzerland)) was transferred onto the UV15 layer and opened lithographically to create 1-μm apertures that connect the channels to the active surface. The transfer of AZ1518 membranes was performed as described previously (12) with some modifications. In brief, AZ1518 was spin-coated onto a plan-parallel, wafer-like PDMS layer of a few millimeters in thickness. After drying in air for 6 min, the layer was readily transferred onto the UV15 substrate with a softbaking step at 60°C for 3 min. After cooling to room temperature, the PDMS was peeled off, leaving the photoresist on the device.

Gradient modeling

The EGF concentration gradients in the various devices described in this article are modeled using computational fluid dynamics to solve the Navier-Stokes and diffusion equations (13). Two structures are modeled; the modified micropipette assay (MA) used to create a steep EGF gradient (10) and the PD presented above. The natures of these geometries lend themselves to different numerical approaches.

The numerical domain of PD (Fig. 3 *A*) consists of a 1-μm aperture that dispenses the EGF solution and extends 20 μm above and 40 μm radially away from the aperture. The symmetry of the chamber allows the problem to be decomposed into radial and angular components, providing a three-dimensional simulation at reduced computational cost. The leftmost boundary of the numerical domain is the axis of rotational symmetry. The top and right boundaries are treated as far-field approximations, given the assumption that at an infinite distance away from the boundary the EGF concentration is zero. These boundary conditions impose limitations of physically correct behavior on the system. The bottommost boundary is treated as an inlet that introduces 1 μM of EGF solution into the computational domain at a proscribed pressure. All remaining boundaries are treated as solid surfaces (walls), which force the fluid to a velocity of zero at the boundary. The numerical domain is filled with a triangular mesh, which resolves features on the domain as small as 20 nm. This design of numerical domain ensures physicality of the solution.

Cell culture

MTLn3 breast carcinoma cells were cultured in Dulbecco modified Eagle medium (DMEM) supplemented with 5% fetal bovine serum and 100 U/mL penicillin and 0.1 mg/mL streptomycin (Invitrogen, Carlsbad, CA). The chamber was set up by adhering the PDMS structure, which defines the chamber walls, onto the wafers (containing the channels and apertures), while using gentle pressure. The MTLn3 breast cancer cells were then trypsinized and seeded at 10^3 cells in 100 μL within the space created by the PDMS. The construct containing the cells was then moved into the metal housing; the PMMA block was placed on top, followed by the lid of the metal

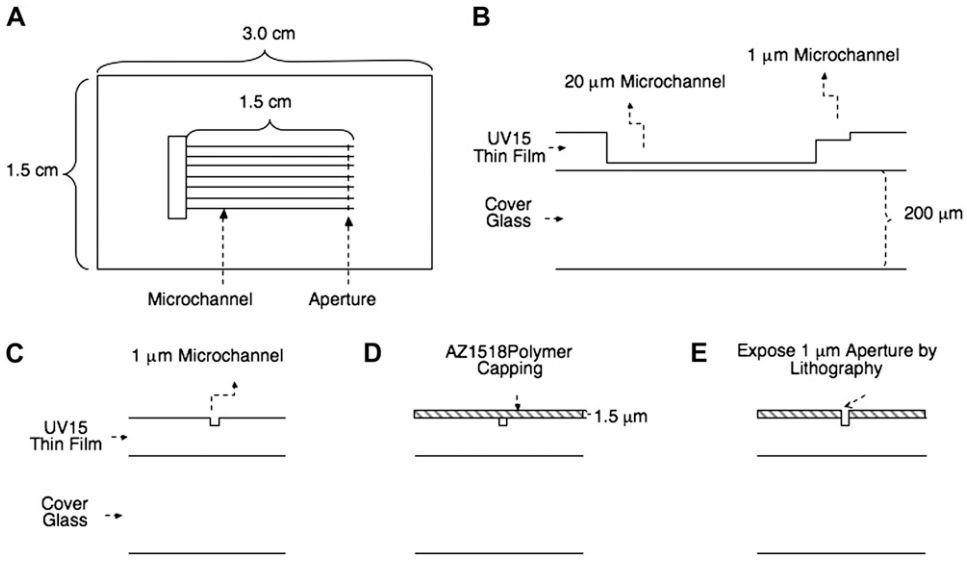

FIGURE 1 Construction of the active surface. (*A*) Top view showing the microchannels and apertures of the microfluidic chip. (*B*) Cross-sectional lateral view illustrating the UV15 layer on a cover glass. A microchannel imprinted on the film by photolithography is also shown. The microchannel measures 20×20 μm in dimension but is reduced to 1 μm in size at one end. (*C*) Cross-sectional frontal view at the 1-μm end of the microchannel. (*D*) Spin-coating of a AZ1818 layer over the microchannel. (*E*) Opening of the AZ1818 by lithography to produce a 1-μm aperture exiting a microchannel.

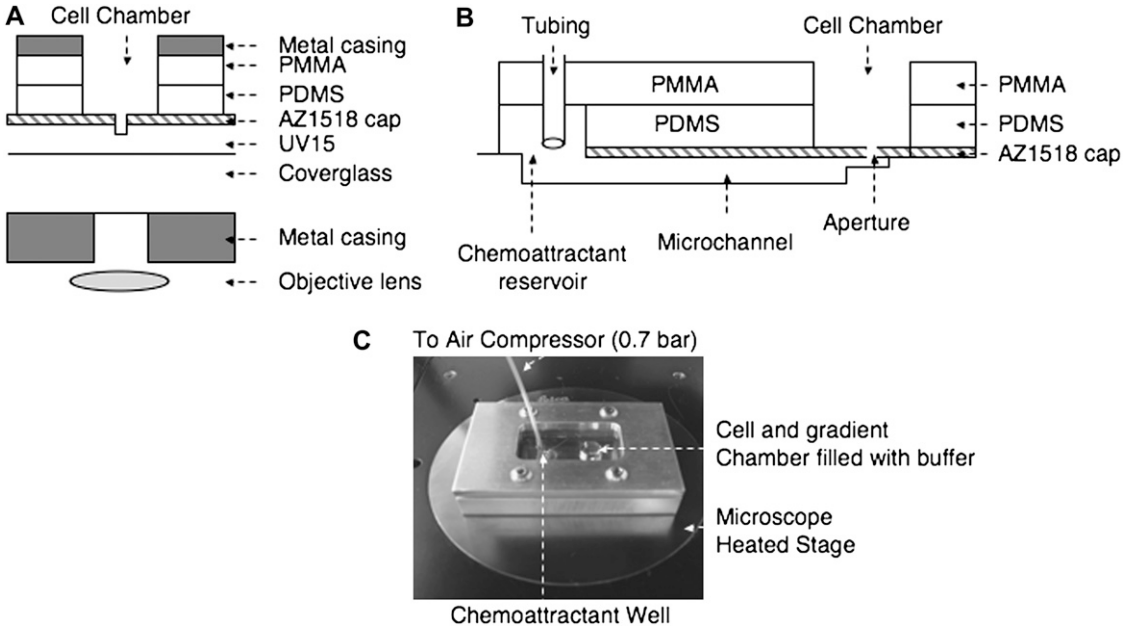

FIGURE 2 Construction of the planar microfluidic device. (*A*) Cross-sectional frontal view illustrating the active AZ1818 surface with a single 1-μm aperture overlying a microchannel imprinted on UV15. The PDMS layer contains two openings of 6 mm in diameter and seals onto the AZ1518 layer. The PDMS openings define the walls of the chamber as shown and the reservoir/inlet (not shown). The PMMA block has an opening at the chamber that superimposes the PDMS opening. The PMMA is rigid and helps compress and seal the layers when encased by the metal housing. The housing contains screws that can be tightened to improve the seal. (*B*) A lateral view in cross section demonstrating that the microchannel opens to an aperture on the AZ1518 surface inside the cell chamber and connects this outlet to the reservoir/inlet on its other end. The PMMA block, which has a plastic tube insert with a 1-mm inner diameter, is placed over the PDMS. The tubing is directed into the reservoir. (*C*) The sealed chamber on a microscope stage. Once sealed, a syringe is used to fill the reservoir with tracer/chemoattractant. The tubing is then connected on the other end to a compressed air outlet. Pressure applied at 0.7 bar at the start of the experiment is sufficient to conduct the tracer/chemoattractant from the reservoir into the microchannels and through the apertures into the buffer-filled chamber.

housing. The structure was secured by tightening screws that compressed the layers within the housing. The cells were incubated at 37°C in a 5% CO_2-regulated incubator for 24 h.

Microfluidics and time-lapse microscopy

The chamber was set up by adhering the PDMS with holes that define the chamber walls onto the active device (containing the channels and apertures) with gentle pressure and by assembling other layers as described above. The chamber was then placed on the heated stage (37°C) of a laser confocal microscope (Leica TSP II; Leica, Ernst-Leitz-Strasse, Germany). Flow was tested using bromophenol blue as a marker and phase contrast microscopy. Imaging of the gradient and cell chemotaxis were performed using fluorescein isothiocyanate (FITC)-conjugated dextran (0.25 mM) alone or together with EGF at 1 μM. The conjugates and factors were placed in the tubing connected to the chamber using a syringe. The tubing was then connected to a compressed air outlet, and the air pressure was increased at the onset of the experiment to 0.7 bar. Time-lapsed sequences were generated by confocal or phase contrast microscopy using a 20× objective at 30-s intervals to record the formation of the gradient and cell activity.

Image analysis

The line drawing feature and intensity measurement functions were used in the public domain, Java-based image processing program developed at the National Institutes of Health (Image J) to obtain intensity values with distance from the opening of the aperture and across the horizontal surface of the chamber. Three separate line intensity measurements were obtained for each frame of the series. The data were transferred to Excel (Microsoft, Redmond, WA); the intensity readings were averaged and plotted as an intensity curve over distance. Directionality measured in terms of cos θ-values and instantaneous speed have been previously described in detail (10). In brief, the directional change of the cell is defined as the shift in its centroid position relative to the direction of the gradient. The outline for each cell was traced, and the change in direction of the cells in degrees (θ) was measured for each frame based on their centroid positions. Cos θ-values were obtained where values close to 1 indicated close reference to the direction of the gradient and values that deviated closer to zero indicated random directions. Instantaneous speed was calculated as the distance between the centroid positions of frame n-1 and frame n divided by the time-lapse interval (30 s) and was the average value obtained for the duration of the assay (5 min).

RESULTS AND DISCUSSION

Physical mechanism

The processes of creating small, high aspect ratio features in thick substrates normally require anisotropic plasma etching, which is expensive and incurs etch bias anomalies (14,15). The method described here, using a thin substrate, works well in the lithographic generation of micrometer-size apertures over microfluidic channels. The requirements for the chamber were to accommodate several microchannels on a transparent, 200-μm thick substrate, and the channels were to be opened by a 1 μm × 1 μm aperture on one end and to connect to a reservoir/inlet at the other end. It was further a requirement that, through pressure, a feeding fluid could be pumped

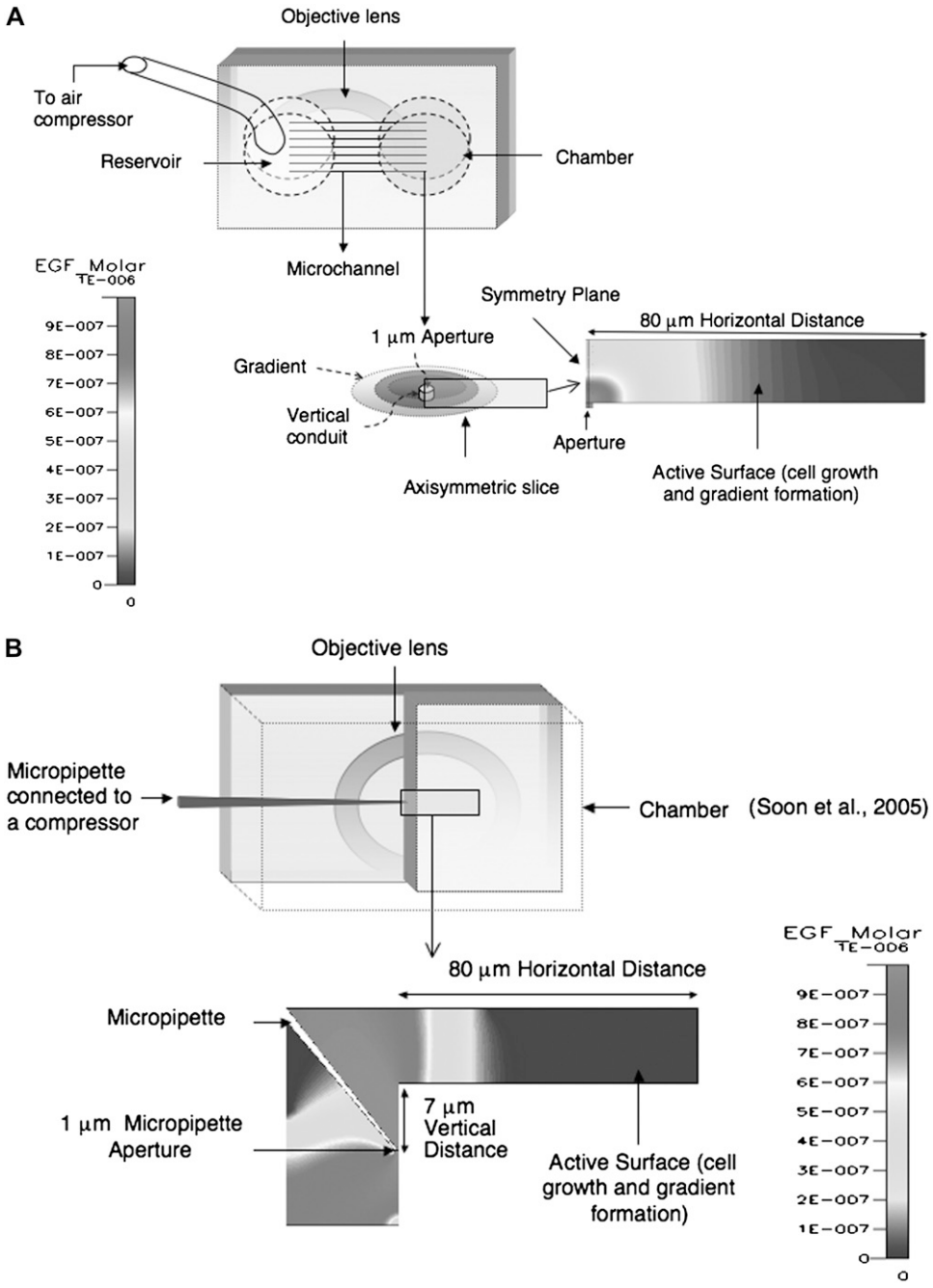

FIGURE 3 Modeling the microfluidic gradient from (*A*) the PD and (*B*) the MA. Both devices operate on the principle of the generation of steep gradients for cellular processes. (*A*) The PD device produces an active horizontal gradient that results from a vertical flow of chemoattractant. Due to rotational symmetry, only an axisymmetric slice was modeled. (*B*) The MA device generates a horizontal gradient from flow delivered at an angle and at a position 7 μm below the active surface. The aperture of the micropipette abuts the side wall of a coverslip on top of which cells are grown. The resulting gradient formed on the active plane is steep. The PD gradient was compared with that produced from MA; the latter was previously shown to stimulate cancer cell chemotaxis. The simulations were performed using the computational fluid dynamics-ACE package (ESI US R&D., Huntsville, AL) to solve the Navier-Stokes and mass diffusion equations on an unstructured tetrahedral gird. A radial coordinate system and a two-dimensional section was used for the PD and MA devices, respectively, as appropriate for their symmetries. The gird places were at least 10 points across the smallest feature of the device (generally 100-nm grid spacing). The solver was iterated until the solution residual differed by less than 1 part in 1000. The results indicate that the simulated gradients for both devices are very similar whereby 1 μM of EGF present in either the PD microchannels or MA micropipette becomes rapidly reduced to physiological levels of 10–50 nM from within 40 μm away from the source.

from the reservoir through the channels to the open tank framed by PDMS walls. The purpose of the aperture is to restrict the flow to create a sharply defined diffusion gradient of the feeding fluid into the water-based tank (Figs. 1 and 2). The adhesion of the AZ1518 layer containing the apertures was excellent throughout the experiment.

Modeled gradients

The model of the micropipette is a two-dimensional cross section through the center pipette. The smallest feature of the numerical domain is resolved; that is, the space between the tip of the pipette and the substrate has at least 20 grid points occupying it. In other words, the 1-μm aperture of the pipette is divided into 1/10 μm grid spacing around the opening of the pipette aperture. The boundaries that lead into free space have outflow boundary conditions, and the walls of the device have no-slip, zero velocity boundary conditions. The aperture of the micropipette is modeled using an inflow boundary condition.

The numerical method solves the standard laminar flow Navier-Stokes equations,

$$\rho\frac{D\mathrm{v}}{Dt} = \nabla\cdot\sigma_{\mathrm{ij}} + \mathrm{f},$$

where

$$\sigma_{\mathrm{ij}} = \begin{pmatrix} \sigma_{\mathrm{xx}} & \tau_{\mathrm{xy}} & \tau_{\mathrm{xz}} \\ \tau_{\mathrm{yx}} & \sigma_{\mathrm{yy}} & \tau_{\mathrm{yz}} \\ \tau_{\mathrm{zx}} & \tau_{\mathrm{zy}} & \sigma_{\mathrm{zz}} \end{pmatrix} = -\begin{pmatrix} p & 0 & 0 \\ 0 & p & 0 \\ 0 & 0 & p \end{pmatrix} + \begin{pmatrix} \sigma_{\mathrm{xx}}+p & \tau_{\mathrm{xy}} & \tau_{\mathrm{xz}} \\ \tau_{\mathrm{yx}} & \sigma_{\mathrm{yy}}+p & \tau_{\mathrm{yz}} \\ \tau_{\mathrm{zx}} & \tau_{\mathrm{zy}} & \sigma_{\mathrm{zz}}+p \end{pmatrix},$$

where the diagonal matrix ρ is the pressure matrix and σ is the viscous stress tensor, which describes the response of the fluid. The fluid (water) is assumed incompressible and Newtonian, which implies the following:

$$\tau = \mu\frac{\partial u}{\partial y,}$$

where μ is the viscosity of the fluid. The diffusions of species is modeled using the diffusivity equation where the species has a diffusion coefficient of D.

The numerical scheme is a discretization of the above equations, solved using finite volume methods with a second-order upwind scheme. The discretization of the geometric domain is tessellated with a triangular mesh, resolving features as cited above.

The 1-μm diameter pipette numerical domain is shown in (Fig. 3 *B*). No symmetry exists as in the case of the modified MA, and so a two-dimensional ''cut'' is taken through the middle of the pipette. For the PD, similar conditions are applied to this geometry as to MA: the outlet boundaries are far-field in nature, the end of the pipette is the inlet for EGF, and all other surfaces are solid walls.

Computer simulations demonstrated that the gradient from the PD system (Fig. 3 *A*) was similar to one generated using a MA (Fig. 3 *B*). The aperture size of the current planar system is 1 μm—the same as the dimension of the bore of the micropipette. The latter was abutted against the wall of a coverslip, 7 μm below the level of the coverslip surface where cells were grown. The MA method was previously shown to create a very steep gradient at the cell surface that was suitable for cancer cell chemotaxis (10). In the current PD set-up, the gradient that was formed at the opening of the aperture was similar in shape and steepness compared to the MA assay. The premise behind both chambers lies in the steep gradient that is created within a 40-μm perimeter around the apertures along the horizontal surface.

Empirical gradients

The flow through the microchannels was tested using India ink and bromophenol blue (S. Fok, P. Domachuk, G. Rosengarten, N. Krause, F. Braet, B. Eggleton, and L. Soon, unpublished observations). To establish the kinetics and steady-state conditions of the gradient, a fluorescent marker, fluorescein-conjugated dextran, was used and a time-lapse sequence was performed to record the intensity of fluorescence over time (Fig. 4). Reconstruction of the movies demonstrated that the gradient was established by around 50 s after pressure application of 0.7 bar (Fig. 4 *B*). Analysis of the change in intensity over distance from the aperture showed that the gradient established was steep and similar to one generated using the MA assay (Fig. 4 *C*), which also recapitulated data obtained from computer simulations (Fig. 3).

Analysis of cell protrusion

Chemotaxis consists of several steps performed by cells in a dynamic, integrated sequence. These steps include the initial detection of chemoattractant through cell surface receptors, the internal polarization of biochemical factors that set the direction of movement, cell protrusion, adhesion, deadhesion, and cell translocation (3). We show that it is possible to monitor the behavior of cancer cells in the first 5 min after EGF stimulation, which provides information about the early chemotaxis steps including protrusion. MTLn3 breast carcinoma cells were seeded overnight onto collagen 1-coated chambers, which were then placed onto the microscope stage for time-lapse microscopy (Fig. 5 *A*). The cells were exposed either to a gradient of EGF or buffer alone, and time-lapsed images were acquired at 30-s intervals. The first 5 min of cell activation were analyzed for directionality and instantaneous speed. Cell directionality was measured as the deviation of the cell's centroid direction relative to the direction of the EGF gradient during the course of the assay (Material and Methods). In the first 5 min after activation, the cancer cells demonstrated directionality preference toward the EGF gradient, as shown by before and after cell contour maps (Fig. 5 *B*) and cos θ measurements (Fig. 5 *C*). As cells move toward the gradient, the value of cos θ will lie close to 1; if the cells move in the opposite direction to that of the gradient, however, cos θ-values veer toward -1. The results show that, in the first 5 min after EGF activation, the cells responded by polarizing toward the gradient (Fig. 5 *B*) and by demonstrating a mean cos θ-value of 0.68 $\pm$ 0.12. This is significantly different from control cells, which showed an average cos θ of 0 $\pm$ 0.26 (Fig. 5 *C*).

Instantaneous speed, calculated as the rate of cell movement between successive cell frames, essentially measured protrusion rates, because the most profound change that occurred in the first 5 min was the spread of the lammellipod at the cell front. The instantaneous speeds measured in the ex-

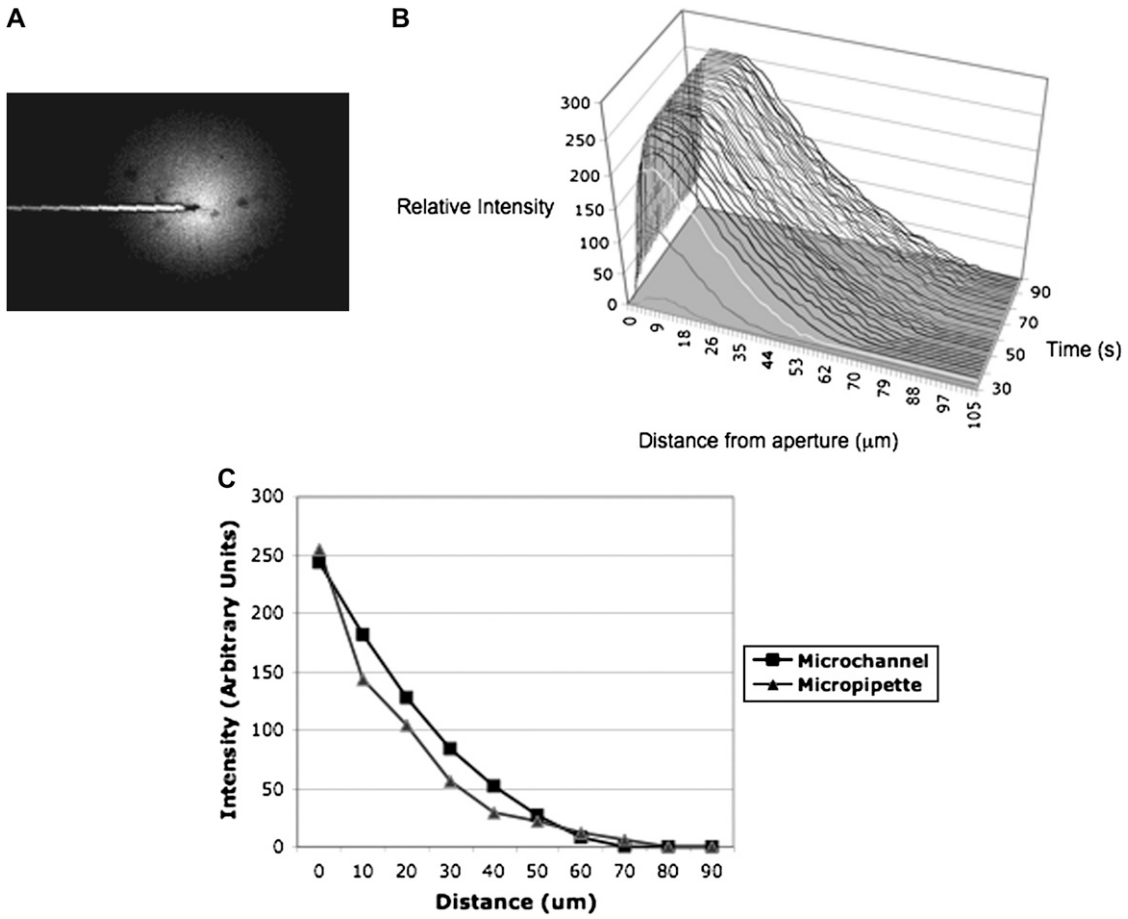

FIGURE 4 Empirical analysis of gradients. (*A*) The reservoir was loaded with filtered FITC-dextran through the tubing, the device was enclosed in the metal encasing, and the whole structure placed on an inverted microscope. The other end of the tubing was connected to a compressed air outlet and pressure was applied at 0.7 bars. The fluorescent dye was observed to travel from the reservoir, across the microchannels, and was released at the apertures. The confocal image shows the release of FITC-labeled dextran and the presence of a gradient around the aperture. (*B*) The speed of gradient formation was analyzed over time from 0 s at the start of pressure induction. Steady-state extrusion was observed by 50 s when the gradient had stabilized at various distances from the aperture, as illustrated by the plateau in the graph. (*C*) The steady-state gradient was compared empirically for both the PD and MD devices. Line intensity measurements were made with distance from the source of the dye over 1 h. The average intensities were plotted against distance, and the graphs show a steep slope for the two gradients indicating that the gradients fall sharply with distance from the source.

periments indicate that cells formed protrusions at a faster rate in the presence of EGF compared to control buffer conditions. The mean of the instantaneous speed, 0.5 ± 0.05 μm/min, is similar to that of published data for cancer cell chemotaxis, 0.57 ± 0.04 μm/min, toward EGF (10).

These results demonstrate that the planar chamber can be used to evaluate the first few steps of chemotaxis that include directional protrusion. It will also be possible to study other early events such as receptor activation and sensing, given the rapid stabilization of the gradient. The ability to perform these studies on amoeboid-like cancer cells such as MTLn3 was previously restricted to single-cell micropipette stimulation at a short distance (10 μm) from the cell over a similar 5-min period (2). The current capability of the PD to image and analyze multiple cells is an advantage over older systems. This functionality is appropriate for investigations on cytoskeletal restructuring and receptor redistribution, such as early events in the process of chemotaxis (16). The use of the current PD chamber can be easily extended to longer chemotaxis assays for the study of individual components/steps of the process and the dynamic chemotaxis cycle itself.

Advantages and some limitations

There are several practical advantages to using the current PD rather than the MA (10). The MA device is not stably bonded; several loose parts are assembled before the experiment. The process involves growing cells separately on glass coverslips, transferring these coverslips onto a glass bottom chamber, and positioning of the micropipette to a distance of 17 μm below the coverslip. In the PD, the assembly process is unnecessary as all the parts are ''built-in''. The cells, for example, are grown in the chamber provided. Similar to the MA device, the chemoattractant is delivered from below the

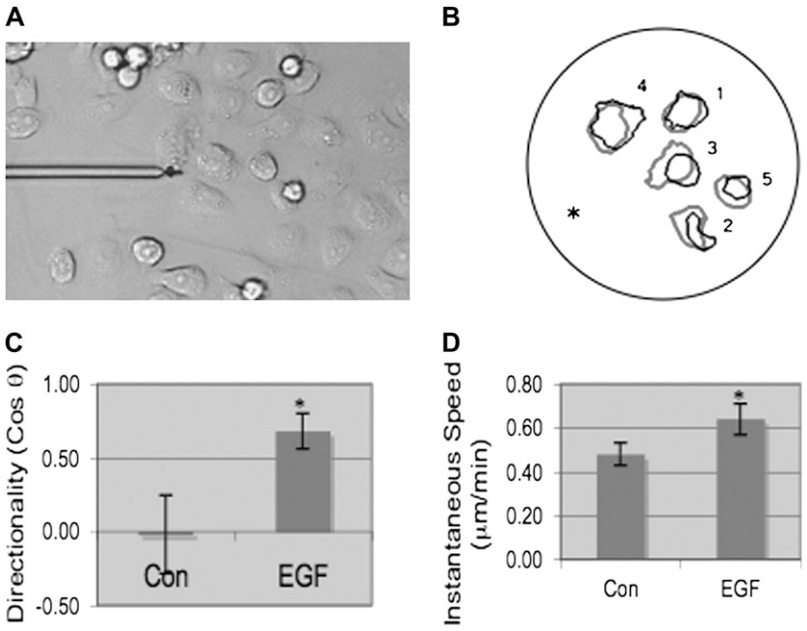

FIGURE 5 Analysis of cell protrusion. MTLn3 breast carcinoma cells were seeded in a chamber coated with 10 μg/mL of collagen I. Time-lapsed microscopy was performed acquiring an image at every 30-s interval. The image stack was analyzed using Image J software to investigate the parameters of cell protrusion. (*A*) Phase contrast image shows cancer cell growth after an overnight incubation at 37°C in a 5% CO_2 incubator. (*B*) Cancer cells demonstrate changes in cell shape after a 5-min exposure to the EGF gradient. This is illustrated by the outline of the cells before (*black contour*) and after EGF activation (*gray contour*). Asterisk indicates position of the aperture and source of EGF in the chamber. (*C*) The experiments were conducted in the absence (*con*) and presence of an EGF gradient (*EGF*) and were analyzed for changes in directionality. This was performed by calculating the cosine of the angle of cell deviance from the direction of the gradient (θ) (Materials and Methods). In the presence of an EGF gradient, cos θ is closer to 1, whereas in the absence of a gradient, cos θ nears zero. This indicates that the cells are more polarized toward the aperture in the presence of an EGF gradient. The asterisk indicates significant difference in a *t*-test analysis ($p < 0.01$); data measure the means of cos θ-values from n = 9 cells. (*D*) Instantaneous speed, which measures the speed of movement between succeeding cell frames, was calculated for control and EGF-treated cells. The data show an increase in instantaneous speed in cells activated in the presence of an EGF gradient compared to control cells. The asterisk indicates significant difference in a *t*-test analysis ($p < 0.05$); data measure mean of cell speed from n = 9 cells. The experiments were performed twice with similar results.

surface of cell growth, occurring through apertures that are, in turn, linked to underlying microchannels. Therefore, there is no need for assembly of the delivery parts, which is unlike the MA device. Furthermore, whereas the MA device is restricted to one micropipette delivery source, the PD device can be configured to have many apertures of different sizes. Multiple apertures are advantageous because this permits simultaneous imaging of multiple events for more efficient collection of statistical information over the entire experiment.

It was discovered that an overnight incubation in solution at 37°C, as required for cell culture, had caused the UV15 layer containing the microchannels to become susceptible to slow separation from the glass substrate. This was observed as small bubbles in the layers. Although this susceptibility did not hinder our experiments, future chambers should be constructed with a different substrate, such as SU8, to overcome the separation problem. Another limitation of the current configuration is the restriction to the use of low NA, 20× objective lenses due to the additional height imposed by the metal casing. Therefore, despite the optimal combined thicknesses of the microchannel and the aperture layers of ~0.17 mm, the use of higher NA lenses is prohibited due to their shorter working distances. However, future devices could be plasma-bonded; such devices would not require the metal encasing and so enable high-resolution light optical imaging. The transparent glass layers permit the use of the device for a variety of optical techniques including fluorescence, phase contrast, and digital interference contrast microscopy.

Although it has not been studied in tumor microenvironments, a steep gradient of factors have been described in vivo and modeled by computer simulations in heart physiology. The premise of the work by Yoshioka et al (17), lies in the EGF secretion by a cardiomyocyte that led to the down-regulation of the gap junction protein, connexin 43, causing the disruption of cell-to-cell communication. Reduced connexin expression is associated with various chronic heart diseases including hypertrophy. The in vivo experiment consisted of nonuniform EGF gene transfer into cardiomyocytes, demonstrating that containment of EGF expression caused hypertrophy in neighboring but not distant cells. These data supported modeling exercises using a model of a cardiomyocyte surrounded by capillaries and extracellular matrix, where it was shown that the capillaries acted as a sink that removed diffused EGF. This action resulted in a sharp gradient of EGF in the cell's vicinity that stimulated only adjacent but not distant cells.

The tumor microenvironment is varied and dynamic but also highly vascularized. Therefore, it is possible that steep gradients are also present in tumors similar to conditions in the heart. These gradients might play an important role in stimulating the chemotaxis and invasion of cancer cells. By inference, high levels of protrusive and migratory behavior of cancer cells have been observed when they are in close proximity to blood vessels and macrophages. Similar to cardiomyocytes that are cultured in vitro (17), sharp gradients are not observed in the in vitro culture of cancer cells due to the lack of a microvasculature architectural system found in vivo. However, with the use of microfluidic technology as

demonstrated in this article, it is possible to create such gradients in vitro that are suitable for the study of cancer cell chemotaxis (18) and other directional processes such as invasion, axon guidance (19), angiogenesis (20), and branching morphogenesis (21) to uncover the molecular regulatory pathways involved.

We gratefully thank Professor John Condeelis (Albert Einstein College of Medicine) for the gift of MTLn3 breast carcinoma cells. The Australian Microscopy and Microanalysis Research Facility, Sydney, Australia, is gratefully acknowledged for the use of its facilities and staff support.

This work was supported by the National Health and Medical Research Council (NHMRC 402510 to L.L.S.), the Australian Research Council (ARC DP0881012 to L.L.S.) and Fluorescent Applications in Biotechnology and Life Sciences.

REFERENCES

1. Devreotes, P., and C. Janetopoulos. 2003. Eukaryotic chemotaxis: distinctions between directional sensing and polarization. *J. Biol. Chem.* 278:20445–20448.
2. Mouneimne, G., V. DesMarais, M. Sidani, E. Scemes, W. Wang, X. Song, R. Eddy, and J. Condeelis. 2006. Spatial and temporal control of cofilin activity is required for directional sensing during chemotaxis. *Curr. Biol.* 16:2193–2205.
3. Soon, L. L. 2007. A discourse on cancer cell chemotaxis: where to from here? *IUBMB Life.* 59:60–67.
4. Abercrombie, M., J. E. Heaysman, and S. M. Pegrum. 1970. The locomotion of fibroblasts in culture. I. Movements of the leading edge. *Exp. Cell Res.* 59:393–398.
5. Condeelis, J., and J. E. Segall. 2003. Intravital imaging of cell movement in tumours. *Nat. Rev. Cancer.* 3:921–930.
6. Wyckoff, J., W. Wang, E. Y. Lin, Y. Wang, F. Pixley, E. R. Stanley, T. Graf, J. W. Pollard, J. Segall, and J. Condeelis. 2004. A paracrine loop between tumor cells and macrophages is required for tumor cell migration in mammary tumors. *Cancer Res.* 64:7022–7029.
7. Zigmond, S. H. 1977. Ability of polymorphonuclear leukocytes to orient in gradients of chemotactic factors. *J. Cell Biol.* 75:606–616.
8. Zicha, D., G. Dunn, and G. Jones. 1997. Analyzing chemotaxis using the Dunn direct-viewing chamber. *Methods Mol. Biol.* 75:449–457.
9. Lin, F., C. M. Nguyen, S. J. Wang, W. Saadi, S. P. Gross, and N. L. Jeon. 2005. Neutrophil migration in opposing chemoattractant gradients using microfluidic chemotaxis devices. *Ann. Biomed. Eng.* 33:475–482.
10. Soon, L., G. Mouneimne, J. Segall, J. Wyckoff, and J. Condeelis. 2005. Description and characterization of a chamber for viewing and quantifying cancer cell chemotaxis. *Cell Motil. Cytoskeleton.* 62:27–34.
11. McDonald, J. C., D. C. Duffy, J. R. Anderson, D. T. Chiu, H. Wu, O. J. Schueller, and G. M. Whitesides. 2000. Fabrication of microfluidic systems in poly(dimethylsiloxane). *Electrophoresis.* 21:27–40.
12. Huang, Y.-M., M. Uppalapati, W. O. Hancock, and T. N. Jackson. 2005. Microfabricated capped channels for biomolecular motor-based transport. *IEEE Transact. Adv. Packaging.* 28:564–570.
13. Lautrup, B. 2005. Physics of Continuous Matter: Exotic and Everyday Phenomena in the Macroscopic World. Institute of Physics Publishing, Bristol, UK.
14. Cotler, T. J., and M. E. Elta. 1990. Plasma-etch technology. *IEE Circuits and Devices Magazine.* 6:38–43.
15. Gottscho, R. A., and C. W. Jurgensen. 1992. Microscopic uniformity in plasma etching. *J. Vac. Sci. Technol. B.* 10:2133–2147.
16. Soon, L., F. Braet, and J. Condeelis. 2007. Moving in the right direction-nanoimaging in cancer cell motility and metastasis. 2007. *Microsc. Res. Tech.* 70:252–257.
17. Yoshioka, J., R. N. Prince, H. Huang, S. B. Perkins, F. U. Cruz, C. MacGillivray, D. A. Lauffenburger, and R. T. Lee. 2005. Cardiomyocyte hypertrophy and degradation of connexin43 through spatially restricted autocrine/paracrine heparin-binding EGF. *Proc. Natl. Acad. Sci. USA.* 102:10622–10627.
18. Mouneimne, G., L. Soon, V. DesMarais, M. Sidani, X. Song, S. C. Yip, M. Ghosh, R. Eddy, J. M. Backer, and J. Condeelis. 2004. Phospholipase C and cofilin are required for carcinoma cell directionality in response to EGF stimulation. *J. Cell Biol.* 166:697–708.
19. Dent, E. W., and F. B. Gertler. 2003. Cytoskeletal dynamics and transport in growth cone motility and axon guidance. *Neuron.* 40:209–227.
20. Soriano, J. V., N. Liu, Y. Gao, Z. J. Yao, T. Ishibashi, C. Underhill, T. R. Burke, Jr., and D. P. Bottaro. 2004. Inhibition of angiogenesis by growth factor receptor bound protein 2-Src homology 2 domain bound antagonists. *Mol. Cancer Ther.* 3:1289–1299.
21. Atabey, N., Y. Gao, Z. J. Yao, D. Breckenridge, L. Soon, J. V. Soriano, T. R. Burke, Jr., and D. P. Bottaro. 2001. Potent blockade of hepatocyte growth factor-stimulated cell motility, matrix invasion and branching morphogenesis by antagonists of Grb2 Src homology 2 domain interactions. *J. Biol. Chem.* 276:14308–14314.